Acoustic Energy Absorption By A Shear Layer †

Sheryl M. Grace [‡]

Aerospace and Mechanical Engineering Department Boston University 110 Cummington St., Boston, MA 02215

ABSTRACT

This paper discusses a method for predicting the frequency bands in which the energy in an acoustic wave created by a test specimen in an open-testsection wind tunnel will be dissipated by the shear layer which forms at the "wall" of the open-test section. For high Reynolds number, subsonic flows the fluid motion inside the tunnel can be modeled as inviscid and a linear analysis of the system can be developed in which the shear layer is modeled as a vortex sheet. Energy absorption occurs at frequencies for which the motion of the vortex sheet is negatively damped. The calculations have been carried out for reduced frequencies from 0 to 10 and Mach numbers from 0 to 0.4. Additionally, the effect of the test section's streamwise length has been examined. The reduced frequency bands in which the acoustic wave created by the test specimen will be damped do not vary for Mach numbers less than 0.2. Above Mach 0.2, the bands begin to spread. The frequency bands also shift as the test section length varies. This shift is correlated to the total time it takes vorticity to convect downstream and the acoustic pulse to travel back upstream.

INTRODUCTION

In this paper, a method is presented for predicting the frequencies at which sound generated by a test specimen in an open-test-section wind tunnel sufficiently perturbs the shear layer, which forms at the boundaries of the test section, such that the

acoustic energy is modified. It is known that a shear layer lying between a source of sound and an acoustic measurement device will affect the measurement. Previous studies by Amiet [1, 2] defined a correction for the shear layer refraction of acoustic emissions from an object located within an open-jet wind tunnel. In addition to refracting the sound, the shear layer can absorb or add energy to the acoustic signals. It is the prediction of this energy modulation which is the focus of the current research.

The geometric set up under consideration consists of an inlet nozzle and an exit nozzle both with cylindrical cross-sections located on either end of an open-test section as shown in Figure 1. An axisymmetric jet of air exiting from a cylindrical nozzle into an open-test section will be influenced by dominant disturbance modes existing in the region around the jet such that the jet shear layer will roll up at this dominant frequency [3]. For unsteady aerodynamic and acoustic experiments performed in an open-test section facility, the test specimen provides the dominant disturbance mode. The response of the jet shear layer to this dominant mode is then two-fold. First, the main shedding of vorticity from the wall edge at the inlet occurs at the dominant frequency. Then, further shedding occurs because of a feedback due to the interaction of the shear layer with the wall edge at the exit.

Physically, the shear layer, and thus the shed vorticity, results from viscosity; however, for high Reynolds number flows, the shear layer can be invisciblly approximated as a vortex sheet. In an inviscible model, vortex shedding from a wall edge is instigated by unsteady disturbances in the flow and can be modeled by imposing the Kutta condition at the wall edge. This vorticity is convected downstream at a speed on the order of the mean flow speed and interacts with the edge of the downstream diffuser

[†]Copyright ©1998 by Sheryl Grace. Published by the Confederation of European Aerospace Societies, with permission.

[‡]Assistant professor, Member AIAA.

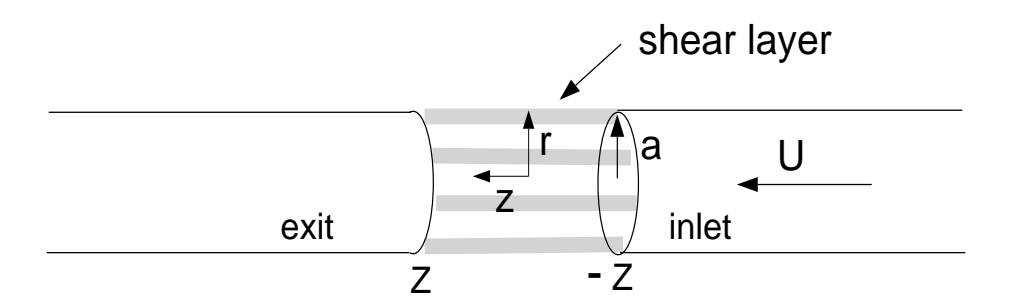


Figure 1: Open-test-section wind tunnel with circular cross section.

wall. Upon interaction, an acoustic pulse is generated which in turn travels back upstream at a speed comparable to the speed of sound. This feedback either enhances the shedding at the upstream wall edge or dampens the shedding. Hence, it affects the motion of the vortex sheet.

The open-test section problem is similar to the problem of grazing flow past a wall aperture; and therefore, the method described in [4] for analyzing the response of a wall aperture in grazing flow to a periodic applied load can be used to perform the current analysis. The method hinges upon analyzing a frequency dependent parameter known as the Rayleigh conductivity $K_R(\omega)$ which is defined as

$$\rho_{\infty} \frac{\partial Q(t)}{\partial t} = -\frac{1}{2\pi} \int_{-\infty}^{\infty} K_R(\omega) \ p_i(\omega) \ e^{-i\omega t} d\omega \quad (1)$$

where Q(t) is the volume flux through the "wall" of the open-test section and $p_i(\omega)$ is the Fourier component with frequency ω of the acoustic pressure disturbance generated by the test specimen. The net volume flux through the boundaries of the test section is proportional to the total displacement of the vortex sheet in the normal direction to the sheet, so that

$$Q = \int v_r dA = \int \frac{D\zeta_r}{Dt} dA \tag{2}$$

where v_r is the radial velocity, ζ_r is the normal displacement, and A is the surface area of the cylindrical "wall" of the open-test section.

If the applied load p_i is periodic in time with frequency ω , and a linearized model of the fluid motion is valid, Eq. (1) can be written as

$$K_R(\omega) = \frac{i\omega \rho_{\infty} \ Q(\omega)}{p_i(\omega)}$$
 (3)

In a real fluid, $K_R(\omega)$ is generally a complex function of the frequency ω , and the energy of an acoustic

sound wave is dissipated by the vortex sheet at a

$$\Pi = -\frac{1}{2} Re(Q^* p_i) \equiv -\frac{Im\{K_R(\omega)\}}{2\rho_\infty \omega} |p_i|^2 \qquad (4)$$

where the asterisk denotes complex conjugate [5]. From this, one notes that if $Im(K_R(\omega)) > 0$ the vortex sheet motion is negatively damped. In this case, the vortex sheet motion grows as it extracts energy from the surrounding flow perturbations. Therefore the acoustic energy of a sound wave generated by a test specimen is damped while the vortex sheet itself may use the energy gained from the original acoustic wave to create another narrow band tone.

In this research, the Rayleigh conductivity is calculated as a function of the reduced frequency, $\bar{\sigma} = \omega a/U$, where a is the radius of the test section and U is the velocity of the fluid in the cylindrical tunnel. Comparisons are made of the conductivity for varying Mach number and for different ratios of test section length to test section diameter.

It is shown that between the reduced frequencies of 0 and 10, there are discrete frequency bands in which acoustic energy would be dissipated by the shear layer. Variations in the Mach number between 0 and 0.2 do not affect the frequency bands, but the magnitude of the conductivity increases with increasing Mach number. As the length to diameter ratio changes, the frequency bands shift accordingly. Because the model is linear, only the reduced frequency bands in which acoustic energy is absorbed can be calculated. To calculate the amplitude of both the energy absorption and the shear layer motion, nonlinear analysis is required. As the length to diameter ratio changes, the frequency bands shift accordingly.

Most of the calculations only use the range of reduced frequency from 0 to 10, i.e. for a wind tunnel operating at Mach .2 or about 200 ft/s, with a ratio of test section lengths of 1.0 the highest reduced

frequency corresponds to a frequency of about 160 Hz. For some anechoic chambers this is at the very low end of the spectrum of measurable frequencies. As such, a method for analyzing the higher reduced frequencies is currently being considered.

MATHEMATICAL FORMULATION

In order to use the Rayleigh conductivity given in Eq. (3) to determine the frequency bands in which energy is absorbed from an acoustic wave, first the normal displacement of the vortex sheet, ζ_r , and the volume flux Q must be calculated. An inviscid, linear model of the fluid dynamics leads to a Helmholtz equation for the velocity potential inside and outside of the cylinder. These velocity potentials are rewritten using Green's theorem in terms of the vortex sheet displacement in the radial direction. The potentials are then linked through the condition of continuity of pressure along the vortex sheet which lies at the "walls" of the open-test section. This leads to a differential-integral equation for the vortex sheet displacement which is solved semi-analytically. Once ζ_r is known, the volume flux Q is easily calculated and thus the Rayleigh conductivity is known. Some of the details of these calculations are included in this section.

The linearized continuity and Euler equations are

$$\frac{D_{\infty} \rho'}{Dt} + \rho_{\infty} \nabla \cdot \vec{u}' = 0 \tag{5}$$

$$\rho_{\infty} \frac{D_{\infty} \vec{u}'}{Dt} = - \nabla p' \tag{6}$$

The convective wave equation with constant coefficients can be transformed into the Helmholtz equation in cylindrical coordinates by using the Prandtl-Glauert transformation $\tilde{r}=\beta_{i,o}r, \tilde{\theta}=\theta, \tilde{z}=z,$ and the Reissner transformation $P=p'e^{i\omega t}e^{iM_{i,o}K_{i,o}\tilde{z}},$ where M is the Mach number, $\beta=\sqrt{1-M^2}, K=\frac{\omega}{c_\infty\beta^2},$ and the subscripts i,o represent inside and outside the cylinder respectively. Additionally, if one notes that

$$\rho_{\infty} \frac{D_{\infty} \Phi}{Dt} = -P \tag{7}$$

where $\Phi = \phi e^{i\omega t} e^{iMKz}$, the Helmholtz equation can be written for the transformed velocity potential Φ as

$$(\tilde{\nabla}^2 + K_{i,o}^2)\Phi = 0 \tag{8}$$

For this problem, the fluid outside the cylinder is not moving and therefore $U_o = 0, U_i = U, M_o = 0, M_i = M, \beta_o = 1.0, \beta_i = \beta$. Because the z variable

is not affected by the Prandtl-Glauert transformation the $\tilde{}$ notation has been dropped in reference to z.

We solve the Helmholtz equation outside and inside the cylinder separately. To do so the Green's function for the cylinder is introduced such that

$$(\tilde{\nabla}^2 + K_{i,o}^2)G = 0, \qquad \frac{\partial G}{\partial \tilde{r}} = \frac{1}{\tilde{r}}\delta(\tilde{r} - \tilde{a})\delta(z - z_0)$$
 (9)

In general a Fourier transform of the Helmholtz equation in the z direction using

$$\int_{-\infty}^{\infty} (\nabla^2 + K^2) G e^{ikz} dz = 0$$
 (10)

$$\int_{-\infty}^{\infty} \frac{\partial G}{\partial \tilde{r}} e^{ikz} dz = \int_{-\infty}^{\infty} \frac{1}{\tilde{r}} \delta(\tilde{r} - \tilde{a}) \delta(z - z_0) e^{ikz} dz \quad (11)$$

results in wave number components of the transformed Green's function \hat{G} satisfying

$$\frac{1}{\tilde{r}}\frac{\partial}{\partial \tilde{r}}\left(\tilde{r}\frac{\partial}{\partial \tilde{r}}\right)\hat{G}+(K^2-k^2)\hat{G}=0$$

$$\frac{\partial \hat{G}}{\partial \tilde{r}}(\tilde{r}, k, \tilde{a}, z_0) = \frac{1}{\tilde{r}} \delta(\tilde{r} - \tilde{a}) e^{ikz_0}$$

Therefore the Green's functions inside and outside the cylinder of radius a respectively are

$$\hat{G}_{i}(\tilde{r}, k, \tilde{a}, z_{0}) = \frac{I_{0}(\sqrt{k^{2} - K_{i}^{2}} \ \tilde{r}) \ e^{ikz_{0}}}{\tilde{a}\sqrt{k^{2} - K_{i}^{2}} \ I_{1}(\sqrt{k^{2} - K_{i}^{2}} \ \tilde{a})}$$

$$\hat{G}_0(r,k,a,z_0) = \frac{-\mathcal{K}_0(\sqrt{k^2 - K_o^2} r) e^{ikz_0}}{a\sqrt{k^2 - K_o^2} \mathcal{K}_1(\sqrt{k^2 - K_o^2} a)}$$

where I_{ν} , \mathcal{K}_{ν} are the modified Bessel functions of order ν . In order to transform the Green's functions back to z space, one must calculate

$$G_{i} = \frac{1}{2\pi} \int_{-\infty}^{\infty} \frac{I_{0}(\sqrt{k^{2} - K_{i}^{2}} \tilde{r}) e^{ik(z_{0} - z)} dk}{\tilde{a}\sqrt{k^{2} - K_{i}^{2}} I_{1}(\sqrt{k^{2} - K_{i}^{2}} \tilde{a})} (12)$$

$$G_o = \frac{1}{2\pi} \int_{-\infty}^{\infty} \frac{-\mathcal{K}_0(\sqrt{k^2 - K_o^2} r) e^{ik(z_0 - z)} dk}{a\sqrt{k^2 - K_o^2} \mathcal{K}_1(\sqrt{k^2 - K_o^2} a)} (13)$$

We are interested in the Green's function for the case of $r \to a$ and z close to z_0 . When one considers the near field of z, the largest contribution to the integrals in (12) and (13) corresponds to large k where

Bessel functions have the property that

$$\lim_{k \to \infty} \frac{I_0(\sqrt{k^2 - K^2}\tilde{a})}{I_1(\sqrt{k^2 - K^2}\tilde{a})} \sim 1$$

$$\lim_{k \to \infty} \frac{K_0(\sqrt{k^2 - K^2}\tilde{a})}{K_1(\sqrt{k^2 - K^2}\tilde{a})} \sim 1$$

The inner Green's function then is

$$G_{i} = \frac{1}{\pi} \int_{0}^{\infty} \frac{\cos(k(z_{0} - z))}{\tilde{a}\sqrt{k^{2} - K_{i}^{2}}} dk$$
$$= -\frac{i}{2\tilde{a}} H_{0}^{(2)}(K_{i}|z_{0} - z|)$$

where $H_0^{(2)} = J_0 - iY_0$ and J and Y are the Bessel functions of order zero [6]. When z is close to z_0 this is further simplified to

$$G_i \sim -\frac{1}{\tilde{a}\pi} \ln(K_i|z_0 - z|) \tag{14}$$

[7]. Similarly it can be shown that

$$G_o \sim +\frac{1}{a\pi} \ln(K_o|z_0 - z|)$$
 (15)

Using these Green's functions one can solve for the potential field inside and outside of the cylinder and take the limit as $r \to a$. For the inner Green's function this gives

$$\Phi_{i}(\tilde{a}, z_{0}) = \int \int G_{i}(\tilde{a}, z, \tilde{a}, z_{0}) \frac{\partial \Phi_{i}(\tilde{a}, z)}{\partial \tilde{\eta}} \tilde{a} d\theta dz$$

$$= 2\pi \tilde{a} \int G_{i}(\tilde{a}, z, \tilde{a}, z_{0}) \frac{\partial \Phi_{i}(\tilde{a}, z)}{\partial \tilde{\eta}} dz (16)$$

and from the definition of Φ it can be shown that

$$\frac{\partial \Phi_i(\tilde{a}, z)}{\partial \tilde{\eta}} = \left(-i\omega + U_i \frac{\partial}{\partial z}\right) \xi_{r_i}(\tilde{a}, z) \tag{17}$$

where ξ_r is the displacement of the vortex sheet in the radial direction (with no β factor taken out and $e^{-i\omega t}$ suppressed).

By substituting these relations into (16), integrating by parts, and rearranging, one can show that

$$\phi_i(\tilde{a}, z) = \frac{2e^{-iMK_iz_0}}{\beta} \left(-i\omega - iMK_iU + U\frac{\partial}{\partial z_0} \right)$$
$$\times \int \ln(K_i|z_0 - z|) \xi_{r_i}(\tilde{a}, z) e^{iMK_iz} dz (18)$$

$$\phi_o(a,z) = 2 (i\omega) \int \ln(K_o|z_0 - z|) \xi_{r_o}(a,z) dz$$
 (19)

Across the vortex sheet the pressure must be continuous. Inside the cylinder there is pressure associated with both the sound from the test specimen (p_i) and the potential flow disturbance from the motion of the vortex sheet as described by Eq. (7). Outside the cylinder there is only pressure associated with the motion of the vortex sheet. Hence the boundary condition can be written as

$$i\omega\phi_o(a,z_0) = \frac{p_i}{\rho_\infty} - \left(-i\omega + U\frac{\partial}{\partial z_0}\right)\phi_i(\tilde{a},z_0)$$

or

$$\frac{p_i}{\rho_{\infty}} = i\omega\phi_o(a, z_0) + \left(-i\omega + U\frac{\partial}{\partial z_0}\right)\phi_i(\tilde{a}, z_0) \quad (20)$$

The matching must occur at the same radial location in physical space. Hence the value of ϕ_i at \tilde{a} is used and value of ϕ_o at a is used. At this point in the field, $\xi_{r_i}(\tilde{a},z) = \xi_{r_o}(a,z)$ and therefore when Eqs. (18) and (19) are substituted into (20), the governing equation becomes

$$\frac{p_i}{2\rho_{\infty}} = -\omega^2 \int \ln(K_o|z_0 - z|) \xi_{r_o} dz
+ \frac{e^{-iMK_i z_0}}{\beta} \left(-\frac{i\omega}{\beta^2} + U \frac{\partial}{\partial z_0} \right)^2
\times \int \ln(K_i|z_0 - z|) \xi_{r_o} e^{iMK_i z} dz$$
(21)

In order to combine the two integrals on the right hand side of Eq. (21) a particular solution to the differential equation

$$\left(U^2 \frac{\partial^2}{\partial z_0^2} - 2i \frac{\omega U}{\beta^2} \frac{\partial}{\partial z_0} - \frac{\omega^2}{\beta^4}\right) f(z_0) =
- \omega^2 \beta e^{iMK_i z_0} \int \ln(K_o |z_0 - z|) \xi_r dz$$
(22)

must be calculated. When $\sigma = \frac{\omega}{U}$ the particular solution can be written as

$$f(z_0) = -\sigma^2 \beta \int \xi_r \left[\frac{e^{iMK_1 z_0}}{-\sigma^2} \left(1 + \ln(K_o | z_0 - z |) \right) + g(z_0 - z) e^{-i\sigma z + i\frac{\sigma}{\beta^2} z_0} (z - z_0 - \frac{i}{\sigma}) \right] dz$$
 (23)

where g is a function whose derivative with respect to z_0 is $\frac{e^{-i\sigma(z_0-z)}}{-i\sigma(z_0-z)}$, i.e.

$$g(z_0 - z) =$$

$$\begin{cases} \frac{\operatorname{Si}(\sigma(z_0 - z)) + i\operatorname{Ci}(\sigma(z_0 - z))}{\sigma} & z_0 - z \ge 0\\ \frac{\operatorname{Si}(\sigma(z_0 - z)) + i\operatorname{Ci}(\sigma(z - z_0))}{\sigma} & z_0 - z \le 0 \end{cases}$$

where Si(x) and Ci(x) are the sine and cosine integral functions

$$\operatorname{Si}(x) = \int_{-\infty}^{x} \frac{\sin(t)}{t} dt$$

$$\operatorname{Ci}(x) = \int_{-\infty}^{x} \frac{\cos(t) - 1}{t} dt$$

All together then the differential integral equation can be written as

$$\beta \frac{p_i}{2\rho_{\infty}} = e^{-iMK_i z_0} \left(\frac{\sigma^2}{\beta^4} + \frac{2i\sigma}{\beta^2} \frac{\partial}{\partial z_0} - \frac{\partial^2}{\partial z_0^2} \right) \times \int \xi_r \operatorname{Ker}(z_0, z) dz$$
(24)

where the kernel is

$$\operatorname{Ker}(z_{0}, z) = -\sigma^{2} \beta \left[\frac{e^{iMK_{i}z_{0}}}{-\sigma^{2}} (1 + \ln(K_{o}|z_{0} - z|)) + g(z_{0} - z)e^{-i\sigma z + i\frac{\sigma}{\beta^{2}}z_{0}} (z - z_{0} - \frac{i}{\sigma}) \right] + \ln(K_{i}|z_{0} - z|)e^{iMK_{i}z}$$
(25)

The differential equation part of the expression can be solved to obtain an integral equation for the displacement of the vortex sheet in the radial direction:

$$\int \xi_r(a,z) \operatorname{Ker}(z_0,z) dz =$$

$$\alpha_1 e^{i\frac{\sigma}{\beta^2} z_0} + \alpha_2 z_0 e^{i\frac{\sigma}{\beta^2} z_0} + \frac{\beta e^{iMK_1 z_0} p_i}{2\rho_{\infty} U^2 \sigma^2}$$
(26)

where $\alpha_{1,2}$ are unknown and the integration can be restricted to the length of the open-test section 2Z as shown in Fig. 1 because $\xi_r = 0$ along the solid walls. If the lengths are nondimensionalized with respect to the radius of the cylindrical-test section a and denoted with an overbar, then the reduced frequency becomes

$$\bar{\sigma} = \frac{\omega a}{U} \tag{27}$$

and the integration is from $-\bar{Z}=-\frac{Z}{a}$ to $\bar{Z}=\frac{Z}{a}$. For convenience ξ_r can be nondimensionalized by

$$\bar{\xi}_r = \frac{\xi_r a 2 \rho_\infty U^2 \sigma^2}{\beta p_i}$$

to o<u>btain</u>

$$\int\limits_{-\bar{Z}}^{\bar{Z}} \bar{\xi}_r(\bar{z}) \operatorname{Ker}(\bar{z}_0 - \bar{z}) d\bar{z} =$$

$$\bar{\alpha}e^{i\bar{\alpha}_1\bar{z}_0} + \bar{z}_0\bar{\alpha}_1e^{i\bar{\alpha}_1\bar{z}_0} + e^{i\frac{M^2}{\beta^2}\bar{\sigma}\bar{z}_0} \tag{28}$$

The integral equation has been solved for $\bar{\xi}_r$ and $\bar{\alpha}_{1,2}$ by imposing the Kutta condition at the leading edge of the test section and using a simple quadrature technique. The interval from $-\bar{Z}$ to \bar{Z} is divided into N equal parts of width dz_j ; the Kutta condition in this discrete setting dictates that $\bar{\xi}_r = 0$ on the two cells nearest the leading edge. Having $\bar{\xi}_r$ specified on two cells allows $\bar{\alpha}_{1,2}$ to be inserted into the list of unknowns in place of the two $\bar{\xi}_r$ values. Once $\bar{\xi}_r$ is known along the length of the test section, the Rayleigh conductivity is calculated by numerical integration

$$K_{R} = \frac{i\omega\rho_{\infty}Q(\omega)}{p_{i}^{o}}$$

$$= \pi a\beta \int_{-\bar{Z}}^{\bar{Z}} \bar{\xi}_{r}(\bar{z})d\bar{z}$$

$$= \pi a\beta \sum_{j=3}^{N} \bar{\xi}_{r_{j}}dz_{j}$$
(29)

RESULTS

The results of the solution to Equations (28) and (29) are described in this section. Typically, the real and negative imaginary parts of the Rayleigh conductivity are plotted as a function of the reduced frequency (or Strouhal number) (i.e., , vs. σ and Δ vs. σ , where $\frac{K_r}{2a} = -i\Delta$.). Here, the Rayleigh conductivity has been nondimensionalized by 2a.

Figure 2 shows the conductivity for a fixed length-to-diameter ratio of 1.0 and increasing Mach numbers from 0.001 to 4.0. The negative imaginary part of the Rayleigh conductivity is shown as the solid line. Figures 2a - 2d confirm that for Mach numbers less than 0.2 the vortex sheet will absorb energy from an acoustic wave for the same set of reduced frequencies. That is, the solid curve dips below zero for approximately the same reduced frequencies. These reduced frequency bands are approximately (1.3, 2.0), (3.55, 4.2), (5.0, 5.65), (6.65, 7.5), (8.25, 8.9).

For a Mach number of 0.3, the first four regimes are similar but the behavior differs past a reduced frequency of eight. Finally, for a Mach number of 0.4, only the first two regimes are similar and the behavior varies past reduced frequencies of about five.

While the frequency regions which correspond to energy absorption of the acoustic wave remain the same for Mach numbers below 0.2, the magnitude of the conductivity differs greatly as the Mach number changes. The change in the magnitude of the conductivity reflects the physically possible vortex sheet motion for the different Mach number cases. When the Mach number approaches zero, as it does for case (a) in Figure 2, this can represent two physical situations. First, the mean flow speed inside the tunnel can be decreasing, $(U \to 0)$. In this case, the Rayleigh conductivity which measures the ratio of the rate of volume flux, based on the vortex sheet motion, to the applied load should vanish. Second, a small Mach number can represent a fixed freestream speed but a very high sound speed. For this case one would again assume that the Rayleigh conductivity would vanish. The test section and the shear layers at the edges of the test section have been modeled using an axisymmetric assumption. Under this assumption if the average motion of the vortex sheet representing the shear layer is inward, the fluid inside the test section must compress. If the speed of sound if very large, the fluid is basically incompressible and therefore the vortex sheet cannot move inward.

The plots in Figure 3 show the effect of the ratio of test section length-to-diameter on the Rayleigh conductivity. At a fixed Mach number of 0.2, the Rayleigh conductivity was calculated for test section length ratios of 0.5, 1.0, and 1.5. The conductivity for these three cases can be explained heuristically. The vortex shedding from the edge of the inlet is producted by the unsteady forcing supplied by the acoustic wave created by the test specimen. The vorticity is convected downstream with a speed on the order of the speed of the fluid inside the tunnel. When the vorticity interacts with the edge of the exit nozzle, another acoustic pulse is generated with travels back upstream at a speed related to the speed of sound. When this pulse interacts with the inlet edge additional vorticity is produced. The frequencies at which the motion of the vortex sheet grows correspond to the frequencies at which the acoustic pulse from downstream produces additional vorticity in phase with the initial shedding.

From a simplified view then, the vorticity in the

wake can be written as a convected disturbance with associated variation

$$e^{i(\omega t - \omega a \bar{z}/U)}$$

The first reduced frequency region in which acoustic energy is absorbed would be centered at

$$\omega = \frac{2\pi U}{a2\bar{Z}}$$

such that the length from inlet edge to exit edge is spanned by one wavelength of the vortex sheet variation. The *n*th region would be centered at the frequency

$$\omega = \frac{2n\pi U}{a2\bar{Z}}$$

This is an overly simplified description because the vortex is not convected with the speed U, and the acoustic pulse takes a finite time to travel and couple with the inlet edge. However, for understanding Fig. 3 the simplified view is helpful. For a shorter-length open-test section the reduced frequency regimes associate with acoustic energy absorption will occur at larger frequencies, i.e. in the simplified explanation

$$\bar{Z}_1 < \bar{Z}_2 \quad \rightarrow \quad \omega_1 > \omega_2$$

Indeed in Figure 3 as the length-to-diameter ratio increases, the first frequency regime of interest is centered about a smaller reduced frequency and the total number of such regimes located between the reduced frequencies of 0 and 10 increases.

The final result presented helps to explain the sharp change in the conductivity seen in Figure 3(c) near a reduced frequency of eight. This same behavior is seen for the case of test section lengthto-diameter ratio of 1.0, at a reduced frequency of 12.0 as shown in Figure 4 (Top) which is an extended version of Fig. 2(d). This sharp change is predicted by calculating the poles of the Rayleigh conductivity. From Equation (1) it is clear that the poles of the conductivity signify frequencies at which the rate of volume flux will be nonzero and physically these frequencies represent the possible selfoscillation frequencies of the system (i.e., the feedback loop does not have to be forced but will occur naturally). When the imaginary part of the pole is in the upper half of the complex plane the system is unstable and the vortex sheet motion will grow, when the imaginary part of the pole is in the lower half of the complex plane, the system is conditionally unstable and would have to be forced at a reduced frequency corresponding to the real part of the pole in order for the vortex sheet motion to grow.

The quantity $|1/K_R(\omega)|$, has been plotted in Fig. 4 (Bottom) for a set of complex reduced frequencies with real part ranging from 0 to 14 and imaginary part ranging from -4 to 10. The poles of the conductivity coincide with the frequencies for which $|1/K_R(\omega_p)| = 0$. Fig. 4 (Bottom) shows many dark regions which indicate possible poles. However, in reality only those regions which have larger areas of dark around them are true poles. The figure shows four poles: at roughly 2.4-0.2i, 5.8+0.5i, 9.0+1.0i, and 11.0 + 1.5i. The real part of these poles are close to the reduced frequencies at which the real part of the Rayleigh conductivity possesses minima. The first pole is stable and the next three are unstable. For the reduced frequencies greater than 12.0, the poles cross back into the stable half of the complex plane, although they are not so obvious in Fig. 4. The peak in the top graph occurs when a pole in the top half plane is very close to the real axis.

The real part of the unstable poles represent the reduced frequencies at which the shear layer spanning from the inlet to the exit may produce tones when the test specimen is not creating an unsteady disturbance [8]. In such circumstances, the initial vortex shedding occurs because of unsteady disturbances in the wall boundary layer upstream of the inlet edge.

CONCLUSIONS

The Rayleigh conductivity for a subsonic opentest-section wind tunnel has been calculated for use in predicting the frequencies at which sound generated by a test specimen located within the test section would be absorbed by the shear layer. It was shown that there are discrete reduced frequency bands for which the shear layer will absorb energy from an acoustic wave, and within these same bands the shear layer motion itself may produce further sound. It was shown that Mach numbers under 0.2 have little affect on the reduced frequency bands in which absorption will occur, but that for Mach numbers of 0.3 and 0.4, the distance between the absorption frequency bands begins to increase. The ratio of test section length-to-diameter also affects the Rayleigh conductivity and the effect further verifies that the dynamics of the vortex sheet is governed by the time it takes a shed vortex to travel from the inlet to the exit plus the time for an acoustic pulse to travel from the exit back to the inlet.

The results shown here correspond to only low

frequency disturbances. However, in practice the frequencies of interest are usually greater than 150 Hz. As such, a method to extend the current analysis to include higher frequencies is under development.

ACKNOWLEDGEMENTS

The author would like to thank Professors Michael Howe and Luigi Morino for their insightful comments regarding the derivation of the Green's function for this application.

REFERENCES

- [1] Amiet, R. K., (1976), "Correction of open-jet wind-tunnel measurements for shear layer refraction," in *Progress in Astronautics and Aeronau*ticsm Vol. 46 (Schwartz, I. R., ed.), pp. 259-280, AIAA.
- [2] Amiet, R. K., (1978), "Refraction of Sound by a Shear Layer," *Journal of Sound and Vibration*, Vol. 58, no. 4, pp. 467-482.
- [3] Hussain, A. K. M. F. and Zaman, K. B. M. Q., (1981), "The 'preferred mode' of the axisymmetric jet," *Journal of Fluid Mechanics*, Vol. 110, pp. 39-71.
- [4] Grace, S. M., Horan, K. P., and Howe, M. S., (1998), "The influence of shape on the Rayleigh conductivity of a wall aperture in the pressure of grazing flow," *Journal of Fluid Structures*. accepted for publication.
- [5] Pierce, A. D., (1989), Acoustics: An Introduction to Its Physical Principles and Applications. New York: Acoustical Society of America.
- [6] Bateman, H., (1954), Tables of Integral Transforms. New York, Toronto, London: McGrall-Hill Book Company, Inc. (Eqs. 1.38, 1.39).
- [7] Abromowitz and Stegun, (1965), Handbook of Mathematical Functions. New York: Dover Publications, Inc. (Eq. 9.1.8).
- [8] Howe, M. S., (1997), "Edge, cavity and aperture tones at very low Mach numbers," *Journal of Fluid Mechanics*, Vol. 330, pp. 61–84.

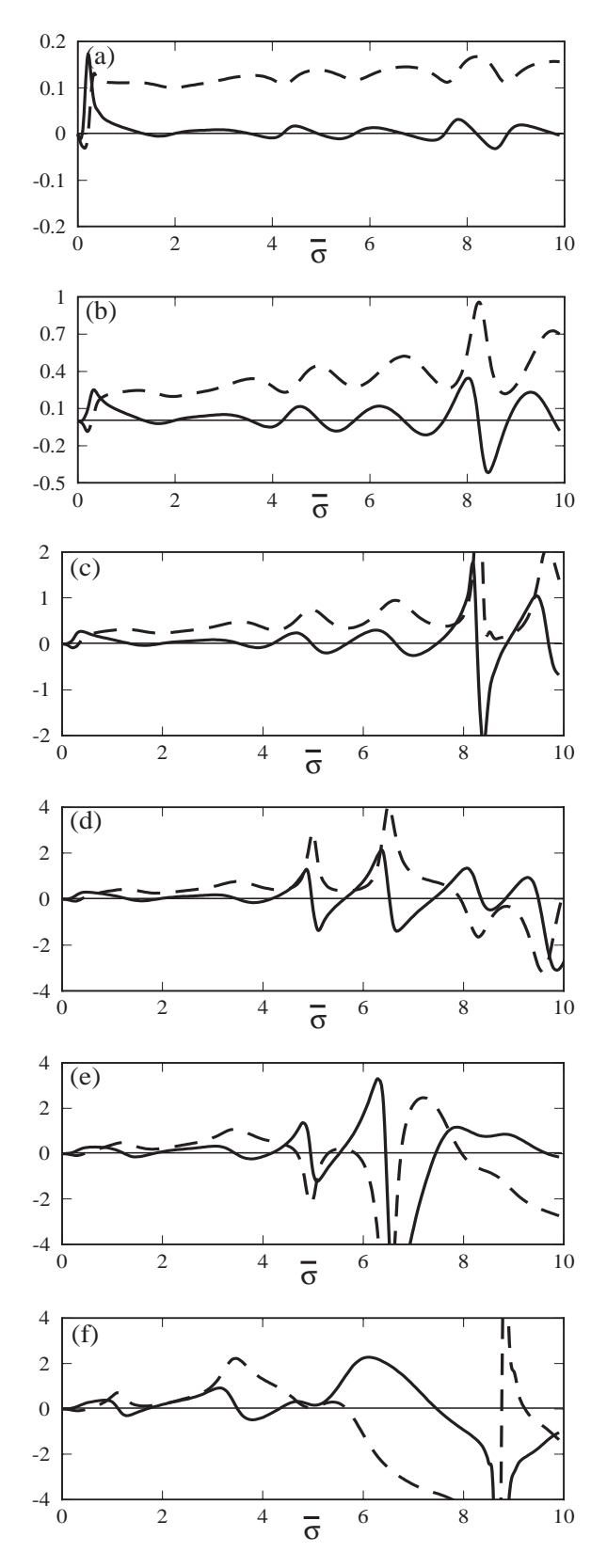


Figure 2: $K_R/2a$: real part (dashed), negative imaginary part (solid). (a) M=0.001, (b) M=0.05, (c) M=0.1, (d) M=0.2, (e) M=0.3, (f) M=0.4.

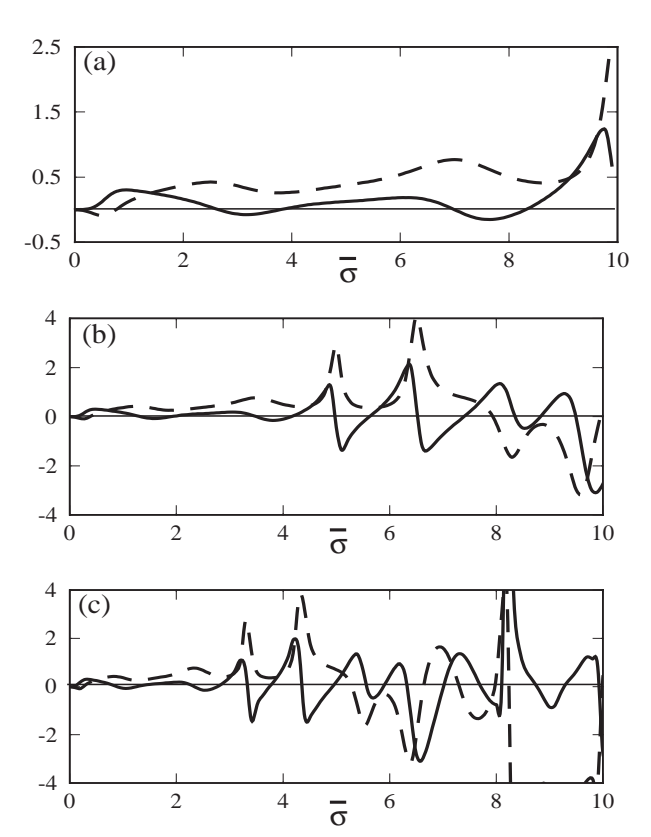


Figure 3: $K_R/2a$: real part (dashed), negative imaginary part (solid). (a) $\bar{Z}=0.5$, (b) $\bar{Z}=1.0$, (c) $\bar{Z}=1.5$.

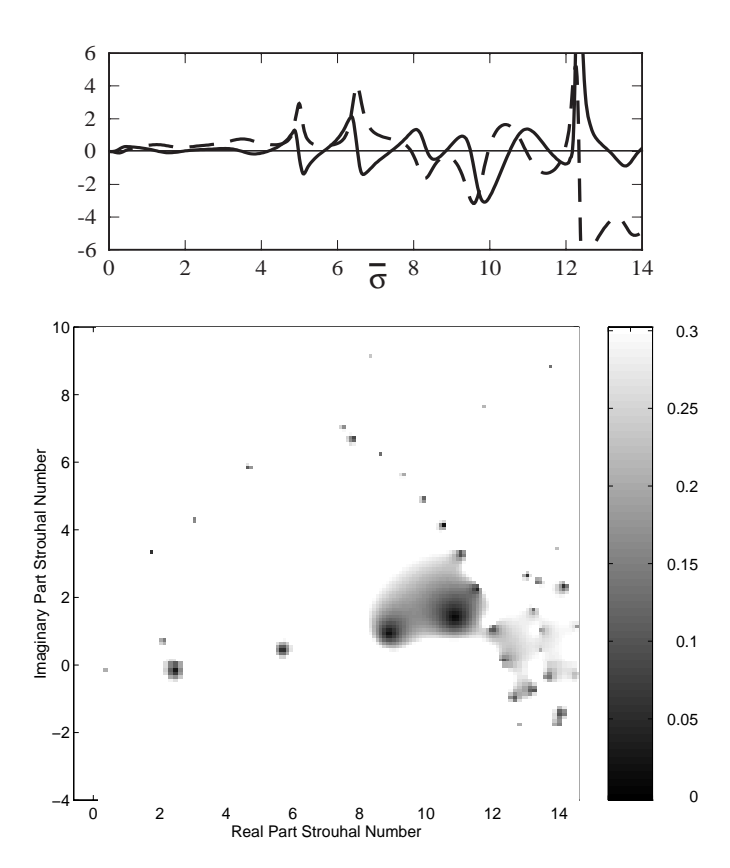


Figure 4: $M=0.2, \bar{Z}=1.0.$ Top: $K_R/2a,$ real part (dashed), negative imaginary part (solid). Bottom: $1/|K_R(\bar{\sigma})|$.